

# Model prediction for temperature dependence of meson pole masses from lattice QCD results on meson screening masses

Masahiro Ishii,<sup>1,\*</sup> Hiroaki Kouno,<sup>2,†</sup> and Masanobu Yahiro<sup>1,‡</sup>

<sup>1</sup>*Department of Physics, Graduate School of Sciences, Kyushu University, Fukuoka 819-0395, Japan*

<sup>2</sup>*Department of Physics, Saga University, Saga 840-8502, Japan*

(Dated: March 23, 2018)

We propose a practical effective model by introducing temperature ( $T$ ) dependence to the coupling strengths of four-quark and six-quark Kobayashi-Maskawa-'t Hooft interactions in the 2+1 flavor Polyakov-loop extended Nambu–Jona-Lasinio model. The  $T$  dependence is determined from LQCD data on the renormalized chiral condensate around the pseudocritical temperature  $T_c^X$  of chiral crossover and the screening-mass difference between  $\pi$  and  $a_0$  mesons in  $T > 1.1T_c^X$  where only the  $U(1)_A$ -symmetry breaking survives. The model well reproduces LQCD data on screening masses  $M_\xi^{\text{scr}}(T)$  for both scalar and pseudoscalar mesons, particularly in  $T \gtrsim T_c^X$ . Using this effective model, we predict meson pole masses  $M_\xi^{\text{pole}}(T)$  for scalar and pseudoscalar mesons. For  $\eta'$  meson, the prediction is consistent with the experimental value at finite  $T$  measured in heavy-ion collisions. We point out that the relation  $M_\xi^{\text{scr}}(T) - M_\xi^{\text{pole}}(T) \approx M_{\xi'}^{\text{scr}}(T) - M_{\xi'}^{\text{pole}}(T)$  is pretty good when  $\xi$  and  $\xi'$  are scalar mesons, and show that the relation  $M_\xi^{\text{scr}}(T)/M_{\xi'}^{\text{scr}}(T) \approx M_\xi^{\text{pole}}(T)/M_{\xi'}^{\text{pole}}(T)$  is well satisfied within 20% error when  $\xi$  and  $\xi'$  are pseudoscalar mesons and also when  $\xi$  and  $\xi'$  are scalar mesons.

PACS numbers: 11.30.Rd, 12.40.-y, 21.65.Qr, 25.75.Nq

## I. INTRODUCTION

Meson masses are fundamental quantities characterizing hadron properties. Temperature ( $T$ ) dependence of meson masses plays an important role in understanding properties of hot-QCD matter, for example, in determining reaction rates of hadron-hadron collisions and dilepton production. In fact,  $T$  dependence of  $\eta'$  and vector mesons was recently measured in heavy-ion collisions [1, 2].

For later convenience, we call the meson mass “meson pole mass” in order to distinguish it from “meson screening mass”. Meson pole and screening masses,  $M_\xi^{\text{pole}}$  and  $M_\xi^{\text{scr}}$ , of  $\xi$  meson are defined by the inverse of the exponential decay of the mesonic correlation function  $\zeta_{\xi\xi}(\tau, \mathbf{x})$  in its temporal  $\tau$ - and spatial  $\mathbf{x}$ -directions, respectively. As seen from the definition,  $M_\xi^{\text{pole}}$  is experimentally measurable, but  $M_\xi^{\text{scr}}$  is not. In first-principle lattice QCD (LQCD) simulations at finite  $T$ , meanwhile,  $M_\xi^{\text{scr}}(T)$  is often calculated instead of  $M_\xi^{\text{pole}}(T)$ , since the spatial lattice size is larger than the temporal one for finite  $T$ . The relation between  $M_\xi^{\text{pole}}(T)$  and  $M_\xi^{\text{scr}}(T)$  is not understood for finite  $T$ , although  $M_\xi^{\text{pole}}(0) = M_\xi^{\text{scr}}(0)$  from the definition.

As already mentioned above, meson screening masses are relatively easier to calculate than meson pole masses in LQCD simulations at finite  $T$ , since the spatial lattice size is larger than the temporal one; see Appendix A for further discussion on the difficulty of meson pole-mass calculations. In fact,  $T$  dependence of light-meson screening masses was recently determined in a wide range  $140 \lesssim T \lesssim 800$  MeV

by 2+1 flavor LQCD simulations with improved (p4) staggered fermions [3]. Meson screening masses are thus available with LQCD simulations, although they are not experimentally measurable.

Meson screening masses are useful in investigating symmetric properties of hot-QCD matter. In principle, one can understand the chiral-symmetry restoration through  $T$  dependence of the mass difference  $\Delta M_{\sigma,\pi}^{\text{scr}}(T) = M_\sigma^{\text{scr}}(T) - M_\pi^{\text{scr}}(T)$  between chiral-partner mesons, say  $\pi$  and  $\sigma$  mesons, and can analyze “the effective  $U(1)_A$ -symmetry restoration” through  $T$  dependence of  $\Delta M_{a_0,\pi}^{\text{scr}}(T) = M_{a_0}^{\text{scr}}(T) - M_\pi^{\text{scr}}(T)$  between  $U(1)_A$ -partner mesons, say  $\pi$  and  $a_0$  mesons. In the operator level,  $U(1)_A$  symmetry is explicitly broken by  $U(1)_A$  anomaly for any  $T$ , but in the expectation-value level the symmetry is restored at high  $T$  by the suppression of topologically-nontrivial gauge configurations responsible for  $U(1)_A$  anomaly. The restoration is called “effective  $U(1)_A$ -symmetry restoration”. For the effective  $U(1)_A$ -symmetry restoration, we cannot define the order parameter clearly, but we may consider the difference  $\Delta M_{\sigma,\pi}^{\text{scr}}(T)$  as an indicator of the restoration. At the present stage, however,  $\Delta M_{a_0,\pi}^{\text{scr}}(T)$  is available but  $\Delta M_{\sigma,\pi}^{\text{scr}}(T)$  is not in LQCD simulations of Ref. [3], because difficult LQCD calculations with the quark-line disconnected diagrams are necessary for  $M_\sigma^{\text{scr}}(T)$ . Parallel discussion may be possible for  $\Delta M_{\sigma,\pi}^{\text{pole}}(T) = M_\sigma^{\text{pole}}(T) - M_\pi^{\text{pole}}(T)$  and  $\Delta M_{a_0,\pi}^{\text{pole}}(T) = M_{a_0}^{\text{pole}}(T) - M_\pi^{\text{pole}}(T)$  if the  $T$  dependence is experimentally measured.

For the 2+1 flavor system composed of light u- and d-quark with the same mass  $m_l$  and s-quark with the mass  $m_s$ , the renormalized chiral condensate

$$\Delta_{l,s}(T) = \frac{\sigma_l(T) - \frac{m_l}{m_s}\sigma_s(T)}{\sigma_l(0) - \frac{m_l}{m_s}\sigma_s(0)} \quad (1)$$

is commonly used as an order parameter (indicator) of the chiral-symmetry restoration [4–6], where  $\sigma_l(T)$  ( $\sigma_s(T)$ ) is

\*ishii@phys.kyushu-u.ac.jp

†kounoh@cc.saga-u.ac.jp

‡yahiro@phys.kyushu-u.ac.jp

the chiral condensate for light quarks (s-quark). The chiral-symmetry restoration is found to be crossover [7] and the pseudocritical temperature  $T_c^X$  is determined to be  $T_c^X = 154 \pm 9$  MeV [5, 6].  $T$  dependence of  $\Delta_{l,s}(T)$  is also obtainable with LQCD, but not directly measurable with experiments.

Physical quantities,  $\Delta_{l,s}(T)$  and  $M_\xi^{\text{scr}}(T)$ , are thus obtainable with LQCD simulations but not with experiments. On the contrary,  $M_\xi^{\text{pole}}(T)$  is experimentally measurable but hard to get with LQCD simulations. If we can predict  $M_\xi^{\text{pole}}(T)$  theoretically from LQCD data on  $\Delta_{l,s}(T)$  and  $M_\xi^{\text{scr}}(T)$ , this makes it possible to compare the  $M_\xi^{\text{pole}}(T)$  predicted from LQCD data with the corresponding experimental data directly. If experimental data are not available for  $M_\xi^{\text{pole}}(T)$  of interest, such a prediction may be helpful in experimental analyses.

As a complementary approach to LQCD simulations, one can consider effective models such as the Nambu–Jona-Lasinio (NJL) model and the Polyakov-loop extended Nambu–Jona-Lasinio (PNJL) model [8–24]. As already mentioned above,  $M_\xi^{\text{pole}}(T)$  are not easy to calculate with LQCD simulations. In addition, if one is interested in physical quantities at finite quark chemical potential  $\mu$ , LQCD simulations face the well-known sign problem, so that LQCD results are concentrated on the  $\mu/T \lesssim 1$  region. For this reason, the phase diagram beyond the region has been discussed and predicted with effective models. In particular, the PNJL model has been applied for many phenomena, since it can treat both chiral and deconfinement transitions. Recently, a Polyakov-loop ( $\Phi$ ) dependent four-quark vertex was introduced to control the correlation between the two transitions [25, 26]. The PNJL model with the entanglement ( $\Phi$ -dependent) four-quark interaction is called the entanglement-PNJL (EPNJL) model [25, 26]. The EPNJL model is quite successful in reproducing LQCD data in the imaginary  $\mu$  region [27, 28] and the real isospin chemical potential region [29] where LQCD is free from the sign problem.

$T$  dependence of  $M_\xi^{\text{pole}}(T)$  for low-lying meson was studied extensively with NJL-type effective models [8, 12, 19, 23, 24, 30]. In spite of the success of NJL-type models in reproducing meson pole masses at  $T = 0$ , it was difficult to calculate  $M_\xi^{\text{scr}}(T)$  with NJL-type models. However, this problem was solved very lately by formulating the meson correlation function carefully in momentum space [31]; see Sec. II C for the detail. For the 2+1 flavor system, NJL-type effective models usually consist of the scalar-type four-quark interaction responsible for the chiral-symmetry restoration and the Kobayashi-Maskawa-'t Hooft (KMT) determinant (six-quark) interaction [32, 33] responsible for the effective  $U(1)_A$ -symmetry restoration. In general, the coupling strength  $G_D$  of the KMT interaction is proportional to the  $T$ -dependent instanton density  $dn_{\text{inst}}(T)$  [34, 35]. For high  $T$ , the instanton density  $dn_{\text{inst}}(T)$  is suppressed by the Debye-type screening [34, 35]. This means that  $G_D$  depends on  $T$ :  $G_D = G_D(T)$ . Very lately,  $T$  dependence of  $G_D(T)$  was determined from LQCD data on  $\Delta M_{a_0,\pi}^{\text{scr}}(T)$  with the EPNJL model [36]. The  $G_D(T)$  thus determined predicts that there is a tricritical point of chiral phase transition in the southwest

direction of the physical point on  $m_l-m_s$  plane. The success of the EPNJL model in reproducing LQCD data is originated in the fact that the coupling strength  $G_S$  of the scalar-type four-quark interaction depends on  $T$  through  $\Phi$ . The EPNJL model is thus essentially equal to the PNJL model with a  $T$ -dependent coupling strength  $G_S = G_S(T)$ , as far as the case of  $\mu = 0$  is concerned.

In this paper, we propose a practical effective model by introducing  $T$ -dependent coupling strengths,  $G_S(T)$  and  $G_D(T)$ , to the 2+1 flavor PNJL model.  $T$  dependence of  $G_S(T)$  is determined from LQCD data on  $T_c^X$  [5, 6] and  $\Delta_{l,s}(T)$  [4], while  $T$  dependence of  $G_D(T)$  is from LQCD data on  $\Delta M_{a_0,\pi}^{\text{scr}}(T)$  [3] in  $T > 1.1T_c^X = 170$  MeV where only the  $U(1)_A$ -symmetry breaking survives [36, 37]. In  $T > 1.04T_c^X = 160$  MeV, this model reproduces LQCD data [3] on  $M_\xi^{\text{scr}}(T)$  for both pseudoscalar mesons  $\pi, K, \eta_{\bar{s}s}$  and scalar mesons  $a_0, \kappa, \sigma_{\bar{s}s}$ . In  $T < 1.04T_c^X = 160$  MeV, the agreement between model results and LQCD data is good for pseudoscalar  $\pi, K$  mesons and pretty good for scalar  $a_0, \kappa, \sigma_{\bar{s}s}$  mesons. For  $\eta_{\bar{s}s}$  meson, the model result overestimates LQCD data by about 10%  $\sim$  30% in  $T < 1.04T_c^X = 160$  MeV, but the deviation becomes small rapidly as  $T$  increases from 160 MeV. The deviation may be related to the fact that the disconnected diagrams are neglected in LQCD calculations. This point is discussed.

Using this practical effective model, we predict meson pole masses  $M_\xi^{\text{pole}}(T)$  for pseudoscalar mesons  $\pi, K, \eta, \eta'$  and scalar mesons  $a_0, \kappa, \sigma, f_0$ . For  $\eta'$  meson, the prediction is compared with the experimental value [1] at finite  $T$  measured in heavy-ion collisions. We show that the relation  $M_\xi^{\text{scr}}(T) - M_\xi^{\text{pole}}(T) \approx M_{\xi'}^{\text{scr}}(T) - M_{\xi'}^{\text{pole}}(T)$  is pretty good when  $\xi$  and  $\xi'$  are scalar mesons, and point out that the relation  $M_\xi^{\text{scr}}(T)/M_{\xi'}^{\text{scr}}(T) \approx M_\xi^{\text{pole}}(T)/M_{\xi'}^{\text{pole}}(T)$  is well satisfied within 20% error when  $\xi$  and  $\xi'$  are pseudoscalar mesons and also when  $\xi$  and  $\xi'$  are scalar mesons. These relations may be useful to estimate  $M_\xi^{\text{pole}}$  for lighter  $\xi$ -meson from  $M_{\xi'}^{\text{pole}}$  and  $M_{\xi'}^{\text{scr}}$  for heavier  $\xi'$ -meson that may be obtainable with state-of-art LQCD simulations.

In Sec. II, we explain the present model and show the methods of evaluating  $M_\xi^{\text{pole}}(T)$  and  $M_\xi^{\text{scr}}(T)$ . Numerical results are shown in Sec. III. Section IV is devoted to a summary.

## II. FORMALISM

### A. Model setting

We consider the 2+1 flavor PNJL model [9–24] and introduce  $T$ -dependent coupling strengths,  $G_S(T)$  and  $G_D(T)$ , for four- and six-quark interactions. The Lagrangian density is

$$\begin{aligned} \mathcal{L} = & \bar{\psi}(i\gamma_\nu D^\nu - \hat{m}_0)\psi + G_S(T) \sum_{a=0}^8 [(\bar{\psi}\lambda_a\psi)^2 + (\bar{\psi}i\gamma_5\lambda_a\psi)^2] \\ & - G_D(T) \left[ \det_{f,f'} \bar{\psi}_f(1 + \gamma_5)\psi_{f'} + \det_{f,f'} \bar{\psi}_f(1 - \gamma_5)\psi_{f'} \right] \\ & - \mathcal{U}(\Phi[A], \bar{\Phi}[A], T), \end{aligned} \quad (2)$$

where the gauge field  $A^\nu$  in  $D^\nu = \partial^\nu + iA^\nu$  is assumed to be  $A^\nu = g\delta_0^\nu(A^0)_a t_a/2 = -ig\delta_0^\nu(A_4)_a t_a/2$  for the gauge coupling  $g$ . The  $\lambda_a(t_a)$  are the Gell-Mann matrices in flavor (color) space,  $\lambda_0 = \sqrt{2/3} \mathbf{I}_F$  for the unit matrix  $\mathbf{I}_F$  in flavor space, and  $\det_{f,f'}$  stands for the determinant in flavor space. In the 2+1 flavor system, the quark fields  $\psi = (\psi_u, \psi_d, \psi_s)^T$  have current quark masses  $\hat{m}_0 = \text{diag}(m_u, m_d, m_s)$  satisfying  $m_s > m_l \equiv m_u = m_d$ .

In the original version of the PNJL model, the coupling strength  $G_D$  of KMT six-quark interaction is constant, but it has been shown very recently in Ref. [36] that  $T$  dependence is necessary for  $G_D$  to explain LQCD data on  $T$  dependence of  $\Delta M_{a_0, \pi}^{\text{scr}}$ , i.e., the  $U(1)_A$ -symmetry restoration. The  $T$ -dependent strength  $G_D(T)$  thus determined is

$$G_D(T) = \begin{cases} G_D(0) & (T < T_1) \\ G_D(0)e^{-(T-T_1)^2/b_1^2} & (T \geq T_1) \end{cases}. \quad (3)$$

$T$  dependence of Eq. (3) is consistent with that of the instanton density  $dn_{\text{inst}}(T)$  [34, 35] for high  $T$ .

It is very likely that  $T$  dependence is necessary also for the coupling strength  $G_S$  of four-quark interaction. We then introduce a  $T$ -dependent coupling strength  $G_S(T)$  of the same function form as  $G_D(T)$ :

$$G_S(T) = \begin{cases} G_S(0) & (T < T_2) \\ G_S(0)e^{-(T-T_2)^2/b_2^2} & (T \geq T_2) \end{cases}. \quad (4)$$

It is possible to determine the parameter set  $(T_1, b_1)$  from LQCD data on  $\Delta M_{a_0, \pi}^{\text{scr}}(T)$  and the set  $(T_2, b_2)$  from LQCD data on  $\Delta_{l,s}(T)$ . The results of this parameter fitting will be shown in Sec. III A. The resultant values are tabulated in Table I. In our previous work [36], we used the EPNJL model with a  $T$ -dependent KMT interaction of form (3). The values of  $T_1$  and  $b_1$  are close to the present ones shown in Table I.

TABLE I: Model parameters in coupling strengths  $G_S(T)$  and  $G_D(T)$ .

$T_1$ [MeV]	$b_1$ [MeV]	$T_2$ [MeV]	$b_2$ [MeV]
121	43.5	131	83.3

In the PNJL model, only the time component  $A_4$  of gauge field  $A_\mu$  is treated as a homogeneous and static background field. In the Polyakov gauge, the Polyakov loop  $\Phi$  and its Hermitian conjugate  $\bar{\Phi}$  are obtained by

$$\Phi = \frac{1}{3} \text{tr}_c(L), \quad \bar{\Phi} = \frac{1}{3} \text{tr}_c(L^*) \quad (5)$$

with the Polyakov-loop operator

$$L = \exp[iA_4/T] = \exp[i \times \text{diag}(A_4^{11}, A_4^{22}, A_4^{33})/T] \quad (6)$$

for real variables  $A_4^{jj}$  satisfying  $A_4^{11} + A_4^{22} + A_4^{33} = 0$ , where the symbol  $\text{tr}_c$  denotes the trace in color space. For the case of  $\mu = 0$  where  $\bar{\Phi} = \Phi$ , one can set  $A_4^{33} = 0$  and determine the others as  $A_4^{22} = -A_4^{11} = \cos^{-1}[(3\Phi - 1)/2]$ .

We take the logarithm-type Polyakov-loop potential of Ref. [18] as  $\mathcal{U}$  that is determined from  $T$  dependence of LQCD data in the pure gauge limit. When the potential is applied to QCD with dynamical quarks, the parameter  $T_0$  included in  $\mathcal{U}$  is used as an adjustable parameter. In the present case, we take  $T_0 = 180$  MeV so that the PNJL model can reproduce 2+1 flavor LQCD data on  $T$  dependence of pion screening mass at  $T \gtrsim T_c^x = 154 \pm 9$  MeV, where the value of  $T_c^x$  is determined with LQCD simulations [5, 6].

Making the mean field approximation (MFA) to Eq. (2), one can obtain the linearized Lagrangian density

$$\mathcal{L}^{\text{MFA}} = \bar{\psi} S^{-1} \psi - U_M - \mathcal{U}(\Phi[A], \bar{\Phi}[A], T), \quad (7)$$

where the quark propagator

$$S = (i\gamma_\nu \partial^\nu - \gamma_0 A^0 - \hat{M})^{-1} \quad (8)$$

depends on the chiral condensates  $\sigma_f = \langle \bar{\psi}_f \psi_f \rangle$  ( $f = u, d, s$ ) through the effective-mass matrix  $\hat{M} = \text{diag}(M_u, M_d, M_s)$  with

$$\begin{aligned} M_u &= m_u - 4G_S(T)\sigma_u + 2G_D(T)\sigma_d\sigma_s, \\ M_d &= m_d - 4G_S(T)\sigma_d + 2G_D(T)\sigma_s\sigma_u, \\ M_s &= m_s - 4G_S(T)\sigma_s + 2G_D(T)\sigma_u\sigma_d. \end{aligned}$$

The mesonic potential  $U_M$  is defined by

$$U_M = 2G_S(T)(\sigma_u^2 + \sigma_d^2 + \sigma_s^2) - 4G_D(T)\sigma_u\sigma_d\sigma_s.$$

Making the path integral over quark fields in the mean-field action, one can get the thermodynamic potential (per unit volume)

$$\begin{aligned} \Omega &= U_M + \mathcal{U} - 2 \sum_{f=u,d,s} \int \frac{d^3\mathbf{p}}{(2\pi)^3} \left[ 3E_{\mathbf{p},f} \right. \\ &+ \frac{1}{\beta} \ln [1 + 3(\Phi + \bar{\Phi}e^{-\beta E_{\mathbf{p},f}})e^{-\beta E_{\mathbf{p},f}} + e^{-3\beta E_{\mathbf{p},f}}] \\ &+ \left. \frac{1}{\beta} \ln [1 + 3(\bar{\Phi} + \Phi e^{-\beta E_{\mathbf{p},f}})e^{-\beta E_{\mathbf{p},f}} + e^{-3\beta E_{\mathbf{p},f}}] \right] \quad (9) \end{aligned}$$

with  $E_{\mathbf{p},f} = \sqrt{\mathbf{p}^2 + M_f^2}$  and  $\beta = 1/T$ . The mean-field variables ( $X = \sigma_l, \sigma_s, \Phi, \bar{\Phi}$ ) are determined by the stationary conditions

$$\frac{\partial \Omega}{\partial X} = 0, \quad (10)$$

where isospin symmetry is assumed for the light-quark sector, i.e.,  $\sigma_l \equiv \sigma_u = \sigma_d$  and  $M_l = M_u = M_d$ .

On the right-hand side of Eq. (9), the first term (vacuum term) diverges. The three-dimensional (3d) momentum-cutoff regularization is often used to avoid the divergence. However, the regularization breaks Lorentz invariance and thereby induces an unphysical oscillation in the spatial correlation function  $\zeta_{\xi\xi}(0, \mathbf{x})$  [38]. In addition, the fundamental relation  $M_\xi^{\text{pole}}(0) = M_\xi^{\text{scr}}(0)$  is not satisfied as a consequence of the Lorentz-symmetry breaking. We then use the Pauli-Villars (PV) regularization [38, 39]. This PV regularization

TABLE II: Model parameters determined from physical quantities at vacuum. Set (A) is the realistic parameter set that is determined from experimental or empirical values at vacuum. In set (B),  $m_l$  and  $m_s$  are slightly changed from set (A) so as to become consistent with the lattice setting ( $m_l/m_s = 1/10$  and  $M_\pi^{\text{pole}}(0) = 176$  MeV) of LQCD simulations of Ref. [3, 4].

	$m_l$ [MeV]	$m_s$ [MeV]	$G_S(0)A^2$	$G_D(0)A^5$	$\Lambda$ [MeV]
set (A) :	8	191	2.72	40.4	660
set (B) :	13	130	2.72	40.4	660

has a parameter  $\Lambda$  with mass dimension; see Sec. II C for further explanation.

Eventually, the present model has five parameters ( $m_l, m_s, G_S(0), G_D(0), \Lambda$ ) in addition to  $T_0, (T_1, b_1)$  and  $(T_2, b_2)$ . The five parameters can be determined from experimental or empirical values at vacuum. The determination of the five parameters should be made before the determination of  $T_0, (T_1, b_1)$  and  $(T_2, b_2)$ . We first assume  $m_l = 8$  MeV and then determine the values of  $(m_s, G_S(0), G_D(0), \Lambda)$  so as to reproduce experimental data,  $f_\pi = 92.4$  MeV,  $M_\pi^{\text{pole}} = 138$  MeV,  $M_K^{\text{pole}} = 495$  MeV and  $M_{\eta'}^{\text{pole}} = 958$  MeV, where  $f_\pi$  is the pion decay constant. The resulting parameter values are shown as set (A) in Table II. When we compare model results with LQCD data, we refit the values of  $m_l$  and  $m_s$  so as to become consistent with the lattice setting. This parameter set is referred to as set (B) in this paper; see Sec. II D for the detail.

Table III shows physical quantities at vacuum calculated with the parameter set (A) of Table II and the corresponding experimental or empirical values. Numbers with asterisk are inputs of the present parameter fitting. The parameter set (A) reproduces available experimental data reasonably well. In addition, the results of set (A) are close to those of the parameter set in Ref. [8] for meson pole masses for  $\eta, a_0, \kappa, \sigma, f_0$ , the mixing angle  $\theta_\eta$  between  $\eta_0$  and  $\eta_8$  states, the mixing angle  $\theta_\sigma$  between  $\sigma_0$  and  $\sigma_8$  states, the effective s-quark mass  $M_s$ , and the kaon decay constant  $f_K$ .

## B. Meson pole masses

We consider pseudoscalar mesons ( $\xi = \pi, K, \eta, \eta'$ ) and scalar ones ( $\xi = a_0, \kappa, \sigma, f_0$ ), and recapitulate the formalism of Refs. [8]. The current operator for  $\xi$  meson is expressed by

$$J_\xi(x) = \bar{\psi}(x) \Gamma_\xi \psi(x) - \langle \bar{\psi}(x) \Gamma_\xi \psi(x) \rangle \quad (11)$$

with  $\Gamma_\xi = \mathbf{I}_C \otimes \Gamma_D \otimes \Gamma_F$ , where  $\mathbf{I}_C$  is the unit matrix in color space. The matrix  $\Gamma_D$  in Dirac space is  $\Gamma_D = \mathbf{I}_D$  for the scalar channel and  $\Gamma_D = i\gamma_5$  for the pseudoscalar channel, where  $\mathbf{I}_D$  is the unit matrix in Dirac space. The matrix  $\Gamma_F$  in

TABLE III: Physical quantities at vacuum calculated with the parameter set (A) of Table II and the corresponding experimental or empirical values. Numbers with asterisk are inputs of the present parameter fitting. Experimental data are taken from Refs. [40, 41]. The effective light-quark mass  $M_l \approx 336$  MeV is estimated from experimental data on baryon magnetic moments [41]. Since we impose the isospin symmetry, we estimate experimental values of averaged pion and kaon masses as  $M_\pi \equiv (M_{\pi^0}^{\text{exp}} + M_{\pi^+}^{\text{exp}} + M_{\pi^-}^{\text{exp}})/3 = (134.97 + 2 \times 139.57)/3 = 138.0$  MeV and  $M_K \equiv (M_{K^0}^{\text{exp}} + M_{K^+}^{\text{exp}} + M_{K^-}^{\text{exp}})/4 = (2 \times 497.61 + 2 \times 493.68)/4 = 495.6$  MeV. Experimental data on the decay constants  $f_\pi$  and  $f_K$  are taken for charged pion and kaon.

	$M_\pi$ [MeV]	$M_K$ [MeV]	$M_{\eta'}$ [MeV]	$f_\pi$ [MeV]	$f_K$ [MeV]
Cal.	138*	495*	958*	92.4*	96.2
Exp.	138.0	495.6	957.8	92.2	110.5
	$M_\eta$ [MeV]	$M_{a_0}$ [MeV]	$M_\kappa$ [MeV]	$M_\sigma$ [MeV]	$M_{f_0}$ [MeV]
Cal.	487	813	1016	674	1185
Exp.	547.8	980±20	800	400~550	980±20
	$\theta_\eta$	$\theta_\sigma$	$M_l$ [MeV]	$M_s$ [MeV]	
Cal.	-7.40°	17.6°	336	544	
Exp.	-11.4°	-	336	-	

flavor space is

$$\Gamma_F = \begin{cases} \lambda_3 & \text{for } \pi, a_0 \\ (\lambda_4 \pm i\lambda_5)/\sqrt{2} & \text{for } K, \kappa \\ \lambda_s & \text{for } \eta_{\bar{s}s}, \sigma_{\bar{s}s} \\ \lambda_{ns} & \text{for } \eta_{\bar{u}l}, \sigma_{\bar{u}l} \end{cases}, \quad (12)$$

where  $\lambda_{ns} = \text{diag}(1, 1, 0)$  and  $\lambda_s = \text{diag}(0, 0, \sqrt{2})$ .

Mesons  $\eta$  and  $\eta'$  ( $\sigma$  and  $f_0$ ) are described as mixed states of  $\eta_{\bar{s}s}$  and  $\eta_{\bar{u}l}$  ( $\sigma_{\bar{s}s}$  and  $\sigma_{\bar{u}l}$ ) states: Namely,

$$\begin{pmatrix} \eta' \\ \eta \end{pmatrix} = O(\theta_\eta^{ls}) \begin{pmatrix} \eta_{\bar{s}s} \\ \eta_{\bar{u}l} \end{pmatrix}, \quad \begin{pmatrix} f_0 \\ \sigma \end{pmatrix} = O(\theta_\sigma^{ls}) \begin{pmatrix} \sigma_{\bar{s}s} \\ \sigma_{\bar{u}l} \end{pmatrix} \quad (13)$$

with the orthogonal matrix  $O(\theta)$

$$O(\theta) = \begin{pmatrix} \cos \theta & \sin \theta \\ -\sin \theta & \cos \theta \end{pmatrix}, \quad (14)$$

where the mixing angle  $\theta_\eta^{ls}$  ( $\theta_\sigma^{ls}$ ) represents the  $\eta_{\bar{s}s}$ - $\eta_{\bar{u}l}$  ( $\sigma_{\bar{s}s}$ - $\sigma_{\bar{u}l}$ ) mixture and is obtained by diagonalizing coupled meson propagators for  $\eta_{\bar{u}l}$  and  $\eta_{\bar{s}s}$  ( $\sigma_{\bar{u}l}$  and  $\sigma_{\bar{s}s}$ ) states [8]. The Fourier transform  $\chi_{\xi\xi'}(q^2)$  of mesonic correlation function  $\zeta_{\xi\xi'}(x) \equiv \langle 0 | T (J_\xi(x) J_{\xi'}^\dagger(0)) | 0 \rangle$  in Minkowski space  $x = (t, \mathbf{x})$  is described by

$$\chi_{\xi\xi'}(q^2) = \chi_{\xi\xi'}(q_0^2, \tilde{q}^2) = i \int d^4x e^{iq \cdot x} \zeta_{\xi\xi'}(x) \quad (15)$$

with (external) momentum  $q = (q_0, \mathbf{q})$ , where  $\tilde{q} = \pm|\mathbf{q}|$  and T stands for the time-ordered product. Using the random-phase (ring) approximation, one can obtain the Schwinger-Dyson equation

$$\chi_{\xi\xi'} = \Pi_{\xi\xi'} + 2 \sum_{\xi''\xi'''} \Pi_{\xi\xi''} G_{\xi''\xi'''} \chi_{\xi'''\xi'} \quad (16)$$

for  $\chi_{\xi\xi'}$ , where  $G_{\xi\xi'}$  is an effective four-quark interaction working between mesons  $\xi$  and  $\xi'$ . The one-loop polarization function  $\Pi_{\xi\xi'}$  is defined by

$$\Pi_{\xi\xi'}(q^2) \equiv (-i) \int \frac{d^4 p}{(2\pi)^4} \text{Tr}(\Gamma_\xi iS(p'+q)\Gamma_{\xi'} iS(p')) \quad (17)$$

with internal momentum  $p = (p_0, \mathbf{p})$ , where  $p' = (p_0 + iA_4, \mathbf{p})$  and the trace Tr is taken in flavor, Dirac and color spaces. The quark propagator  $S(p)$  is diagonal in flavor space:  $S(p) = \text{diag}(S_u, S_d, S_s)$ . The polarization function  $\Pi_{\xi\xi'}(q^2)$  can be classified with quark and anti-quark flavors  $f$  and  $f'$  as

$$\begin{aligned} \Pi_S^{ff'} &= (-2i) \int \frac{d^4 p}{(2\pi)^4} \text{tr}_{c,d}(iS_f(p'+q)iS_{f'}(p')) \\ &= 4i[I_1^f + I_2^{f'} - \{q^2 - (M_f + M_{f'})^2\} I_3^{ff'}] \end{aligned} \quad (18)$$

for the scalar mesons and

$$\begin{aligned} \Pi_P^{ff'} &= (-2i) \int \frac{d^4 p}{(2\pi)^4} \text{tr}_{c,d}((i\gamma_5)iS_f(p'+q)(i\gamma_5)iS_{f'}(p')) \\ &= 4i[I_1^f + I_2^{f'} - \{q^2 - (M_f - M_{f'})^2\} I_3^{ff'}] \end{aligned} \quad (19)$$

for pseudoscalar mesons, where the trace  $\text{tr}_{c,d}$  is taken in color and Dirac spaces and

$$I_1^f = \int \frac{d^4 p}{(2\pi)^4} \text{tr}_c \left[ \frac{1}{p'^2 - M_f^2} \right], \quad (20)$$

$$I_2^f = \int \frac{d^4 p}{(2\pi)^4} \text{tr}_c \left[ \frac{1}{(p'+q)^2 - M_f^2} \right], \quad (21)$$

$$I_3^{ff'} = \int \frac{d^4 p}{(2\pi)^4} \text{tr}_c \left[ \frac{1}{\{p'^2 - M_f^2\} \{(p'+q)^2 - M_{f'}^2\}} \right]. \quad (22)$$

For finite  $T$ , the corresponding equations are obtained by the replacement

$$\begin{aligned} p_0 &\rightarrow i\omega_n = i(2n+1)\pi T, \\ \int \frac{d^4 p}{(2\pi)^4} &\rightarrow iT \sum_{n=-\infty}^{\infty} \int \frac{d^3 \mathbf{p}}{(2\pi)^3}. \end{aligned} \quad (23)$$

Here we explain the PV regularization for the thermodynamic potential  $\Omega$  of Eq. (9) and the three integrals  $I_1^f, I_2^f, I_3^{ff'}$ . For convenience, we divide  $\Omega$  into  $\Omega = U_M + \mathcal{U} + \sum_{f=u,d,s} \Omega_F(M_f)$ , and represent  $I_1^f$  and  $I_2^f$  by  $I(M_f)$  and  $I_3^{ff'}$  by  $I_{ff'}(M_f, M_{f'})$ . In the PV scheme, the functions

$\Omega_F(M_f)$ ,  $I(M_f)$  and  $I_{ff'}(M_f, M_{f'})$  are regularized as

$$\begin{aligned} \Omega_F^{\text{reg}}(M_f) &= \sum_{\alpha=0}^2 C_\alpha \Omega_F(M_{f;\alpha}), \\ I^{\text{reg}}(M_f) &= \sum_{\alpha=0}^2 C_\alpha I(M_{f;\alpha}), \\ I_{ff'}^{\text{reg}}(M_f, M_{f'}) &= \sum_{\alpha=0}^2 C_\alpha I_{ff'}(M_{f;\alpha}, M_{f';\alpha}), \end{aligned} \quad (24)$$

where  $M_{f;0} = M_f$  and the  $M_{f;\alpha}$  ( $\alpha = 1, 2$ ) mean masses of auxiliary particles. The parameters  $M_{f;\alpha}$  and  $C_\alpha$  should satisfy the condition  $\sum_{\alpha=0}^2 C_\alpha = \sum_{\alpha=0}^2 C_\alpha M_{f;\alpha}^2 = 0$  to remove the quartic, the quadratic and the logarithmic divergence in  $I_1, I_2, I_3^{ff'}$ , and  $\Omega_F$ . Logarithmic divergence partially remains in  $\Omega_F^{\text{reg}}(M_f)$  even after the subtraction of Eq. (24), but the term does not depend on the mean-field variables ( $\sigma_l, \sigma_s, \Phi, \bar{\Phi}$ ) and is irrelevant to the determination of mean-field variables for any  $T$ . Therefore we can simply drop the term. We assume  $(C_0, C_1, C_2) = (1, 1, -2)$  and  $(M_{f;1}^2, M_{f;2}^2) = (M_f^2 + 2\Lambda^2, M_f^2 + \Lambda^2)$ , following Ref. [42]. We keep the parameter  $\Lambda$  finite even after the subtraction (24), since the present model is non-renormalizable.

### 1. $\pi, a_0, K, \kappa$ mesons

For  $\xi = \pi, a_0, K$  and  $\kappa$ , the effective four-quark interactions  $G_{\xi\xi'}$  and the polarization functions  $\Pi_{\xi\xi'}$  are diagonal, i.e.,  $G_{\xi\xi'} = G_\xi \delta_{\xi\xi'}$ ,  $\Pi_{\xi\xi'} = \Pi_\xi \delta_{\xi\xi'}$ , because of isospin symmetry in the light-quark sector and the random-phase approximation. One then can easily get the solution to the Schwinger-Dyson equation (16) as

$$\chi_{\xi\xi} = \frac{\Pi_\xi}{1 - 2G_\xi \Pi_\xi} \quad (25)$$

for  $\xi = \pi, a_0, K$  and  $\kappa$ , where the effective couplings  $G_\xi$  are defined by

$$G_{a_0} = G_S(T) + \frac{1}{2} G_D(T) \sigma_s, \quad (26)$$

$$G_\pi = G_S(T) - \frac{1}{2} G_D(T) \sigma_s, \quad (27)$$

$$G_\kappa = G_S(T) + \frac{1}{2} G_D(T) \sigma_l, \quad (28)$$

$$G_K = G_S(T) - \frac{1}{2} G_D(T) \sigma_l \quad (29)$$

and the one-loop polarization functions  $\Pi_\xi$  are written by

$$\Pi_{a_0} = \Pi_S^l, \quad \Pi_\pi = \Pi_P^l, \quad \Pi_\kappa = \Pi_S^s, \quad \Pi_K = \Pi_P^s. \quad (30)$$

The meson pole mass  $M_\xi^{\text{pole}}$  is a pole of  $\chi_{\xi\xi}(q_0^2, \tilde{q}^2)$  in the complex  $q_0$  plane. Taking the rest frame  $q = (q_0, \mathbf{0})$  for convenience, one can get the equation

$$[1 - 2G_\xi \Pi_\xi(q_0^2, 0)]|_{q_0=M_\xi^{\text{pole}} - i\Gamma_\xi/2} = 0 \quad (31)$$

for  $M_\xi^{\text{pole}}$ , where  $\Gamma_\xi$  is the decay width to  $q\bar{q}$  continuum. The  $M_\xi^{\text{pole}}$  and  $\Gamma_\xi$  are obtained numerically by searching for the  $q_0$  satisfying Eq. (31). Here we take the approximation  $\Gamma_\xi/M_\xi^{\text{pole}} \ll 1$ , following Ref. [12].

## 2. $\eta, \eta', \sigma, f_0$ mesons

The pole masses of  $\eta$  and  $\eta'$  ( $\sigma$  and  $f_0$ ) mesons are obtained by solving the coupled-channel equations (16) for  $\eta_{\bar{l}l}$  and  $\eta_{\bar{s}s}$  ( $\sigma_{\bar{l}l}$  and  $\sigma_{\bar{s}s}$ ). It is convenient to express the correlation functions  $\chi_{\xi\xi'}$  with the matrix

$$\chi_\xi = \begin{pmatrix} \chi_{\xi_{\bar{s}s}\xi_{\bar{s}s}} & \chi_{\xi_{\bar{s}s}\xi_{\bar{l}l}} \\ \chi_{\xi_{\bar{l}l}\xi_{\bar{s}s}} & \chi_{\xi_{\bar{l}l}\xi_{\bar{l}l}} \end{pmatrix} \quad (\xi = \eta, \sigma). \quad (32)$$

The Schwinger-Dyson equation for  $\chi_\xi$  is obtained from Eq. (16) as

$$\chi_\xi = \mathbf{\Pi}_\xi + 2\mathbf{\Pi}_\xi \mathbf{G}_\xi \chi_\xi \quad (33)$$

with

$$\mathbf{G}_\xi = \begin{pmatrix} G_{\xi_{\bar{s}s}\xi_{\bar{s}s}} & G_{\xi_{\bar{s}s}\xi_{\bar{l}l}} \\ G_{\xi_{\bar{l}l}\xi_{\bar{s}s}} & G_{\xi_{\bar{l}l}\xi_{\bar{l}l}} \end{pmatrix}, \quad \mathbf{\Pi}_\xi = \begin{pmatrix} \Pi_{\xi_{\bar{s}s}} & 0 \\ 0 & \Pi_{\xi_{\bar{l}l}} \end{pmatrix}. \quad (34)$$

The solution to Eq. (33) is

$$\chi_{\xi_{\bar{s}s}\xi_{\bar{s}s}} = \frac{(1 - 2G_{\xi_{\bar{l}l}\xi_{\bar{l}l}}\Pi_{\xi_{\bar{l}l}})\Pi_{\xi_{\bar{s}s}}}{\det[\mathbf{I} - 2\mathbf{\Pi}_\xi \mathbf{G}_\xi]}, \quad (35)$$

$$\chi_{\xi_{\bar{l}l}\xi_{\bar{l}l}} = \frac{(1 - 2G_{\xi_{\bar{s}s}\xi_{\bar{s}s}}\Pi_{\xi_{\bar{s}s}})\Pi_{\xi_{\bar{l}l}}}{\det[\mathbf{I} - 2\mathbf{\Pi}_\xi \mathbf{G}_\xi]}, \quad (36)$$

$$\chi_{\xi_{\bar{s}s}\xi_{\bar{l}l}} = \chi_{\xi_{\bar{l}l}\xi_{\bar{s}s}} = \frac{2G_{\xi_{\bar{l}l}\xi_{\bar{s}s}}\Pi_{\xi_{\bar{s}s}}\Pi_{\xi_{\bar{l}l}}}{\det[\mathbf{I} - 2\mathbf{\Pi}_\xi \mathbf{G}_\xi]}, \quad (37)$$

where  $\mathbf{I}$  is the unit matrix and the determinant  $\det$  is taken in the  $\xi_{\bar{l}l}$  and  $\xi_{\bar{s}s}$  channels. The matrix elements of  $\mathbf{G}_\eta$  and  $\mathbf{G}_\sigma$  are explicitly obtained by

$$\begin{aligned} G_{\eta_{\bar{s}s}\eta_{\bar{s}s}} &= G_S(T), \quad G_{\eta_{\bar{l}l}\eta_{\bar{l}l}} = G_S(T) + \frac{1}{2}G_D(T)\sigma_s, \\ G_{\eta_{\bar{s}s}\eta_{\bar{l}l}} &= G_{\eta_{\bar{l}l}\eta_{\bar{s}s}} = \frac{\sqrt{2}}{2}G_D(T)\sigma_l, \\ G_{\sigma_{\bar{s}s}\sigma_{\bar{s}s}} &= G_S(T), \quad G_{\sigma_{\bar{l}l}\sigma_{\bar{l}l}} = G_S(T) - \frac{1}{2}G_D(T)\sigma_s, \\ G_{\sigma_{\bar{s}s}\sigma_{\bar{l}l}} &= G_{\sigma_{\bar{l}l}\sigma_{\bar{s}s}} = -\frac{\sqrt{2}}{2}G_D(T)\sigma_l, \end{aligned} \quad (38)$$

and those of  $\mathbf{\Pi}_\eta, \mathbf{\Pi}_\sigma$  are by

$$\Pi_{\sigma_{\bar{l}l}} = \Pi_S^{ll}, \quad \Pi_{\sigma_{\bar{s}s}} = \Pi_S^{ss}, \quad (40)$$

$$\Pi_{\eta_{\bar{l}l}} = \Pi_P^{ll}, \quad \Pi_{\eta_{\bar{s}s}} = \Pi_P^{ss}. \quad (41)$$

The masses of  $\eta$  and  $\eta'$  ( $\sigma$  and  $f_0$ ) are determined as poles of  $\chi_\eta$  ( $\chi_\sigma$ ), that is, as zero points of the determinant in Eqs. (35)-(37):

$$\det[\mathbf{I} - 2\mathbf{\Pi}_\xi(q_0^2, 0) \mathbf{G}_\xi] \Big|_{q_0=M_\xi^{\text{pole}} - i\Gamma_\xi/2} = 0. \quad (42)$$

Two poles are found in the complex  $q_0$  plane. The lighter and heavier pole masses correspond to  $\eta$  and  $\eta'$  ( $\sigma$  and  $f_0$ ) meson masses, respectively.

## C. Meson screening masses

We first show the reason why the derivation of  $M_\xi^{\text{scr}}(T)$  was difficult in NJL-type effective models before the work of Ref. [31], and next recapitulate the method of Ref. [31] and extend it from single-channel systems to multi-channel systems. The  $M_\xi^{\text{scr}}$  is defined with the spatial correlator  $\zeta_{\xi\xi}(0, \mathbf{x})$  in the long-distance limit ( $r = |\mathbf{x}| \rightarrow \infty$ ):

$$M_\xi^{\text{scr}} = - \lim_{r \rightarrow \infty} \frac{d \ln \zeta_{\xi\xi}(0, \mathbf{x})}{dr}, \quad (43)$$

where

$$\zeta_{\xi\xi}(0, \mathbf{x}) = \frac{1}{4\pi^2 i r} \int_{-\infty}^{\infty} d\tilde{q} \tilde{q} \chi_{\xi\xi}(0, \tilde{q}^2) e^{i\tilde{q}r}. \quad (44)$$

Equation (44) has two problems, when the  $\tilde{q}$  integration is performed. The first problem stems from the regularization taken. As already mentioned in Sec. II A, the 3d momentum cutoff is commonly used, but it breaks Lorentz invariance even in  $T = 0$ . This induces an unphysical oscillation in  $\zeta_{\xi\xi}(0, \mathbf{x})$  at large  $r$  [38]. We can easily solve this problem by using the PV regularization. This is the reason why we take the PV regularization in this paper. As easily found from Eq. (44), direct numerical calculations of the  $\tilde{q}$  integration are quite difficult at large  $r$  because of highly oscillation of the integrand. This is the second problem. In order to solve this problem, one can consider analytic continuation of  $\chi_{\xi\xi}(0, \tilde{q}^2)$  to the complex  $\tilde{q}$  plane. In general, the integration can be made easily with the Cauchy's integral theorem. However, the complex function  $\chi_{\xi\xi}(0, \tilde{q}^2)$  has logarithmic cuts in the vicinity of the real  $\tilde{q}$  axis [38]. This demands quite time-consuming numerical calculations to evaluate the contribution of logarithmic cuts [38]. In our previous works [31, 36], we showed that these logarithmic cuts are not physical and avoidable by taking the Matsubara summation over  $n$  after the  $\mathbf{p}$  integration in Eq. (23). Consequently, we obtain the regularized function  $I_{3,\text{reg}}^{ff'}$  as an infinite series of analytic functions:

$$\begin{aligned} I_{3,\text{reg}}^{ff'}(0, \tilde{q}^2) &= iT \sum_{j=1}^{N_c} \sum_{n=-\infty}^{\infty} \sum_{\alpha=0}^2 C_\alpha \\ &\times \int \frac{d^3\mathbf{p}}{(2\pi)^3} \left[ \frac{1}{\mathbf{p}^2 + \mathcal{M}_f^2} \frac{1}{(\mathbf{p} + \mathbf{q})^2 + \mathcal{M}_{f'}^2} \right] \\ &= \frac{iT}{2\pi^2} \sum_{j,n,\alpha} C_\alpha \int_0^1 dx \int_0^\infty dk \\ &\times \frac{k^2}{[k^2 + (x-x^2)\tilde{q}^2 + (1-x)\mathcal{M}_f^2 + x\mathcal{M}_{f'}^2]^2} \\ &= \frac{T}{8\pi\tilde{q}} \sum_{j,n,\alpha} C_\alpha \text{Log} \left( \frac{\mathcal{M}_f + \mathcal{M}_{f'} + i\tilde{q}}{\mathcal{M}_f + \mathcal{M}_{f'} - i\tilde{q}} \right) \end{aligned} \quad (45)$$

with

$$\mathcal{M}_f(T) = \sqrt{M_{f,\alpha}^2 + \{(2n+1)\pi T + A_4^{jj}\}^2}, \quad (46)$$

where ‘‘Log’’ denotes the principle value of the logarithm. The function  $iI_{3,\text{reg}}^{ff'}$  is real for real  $\tilde{q}$ , when  $q_0 = 0$ . This means that mesons do not decay into a quark and an antiquark. The function  $I_{3,\text{reg}}^{ff'}$  is obtained as an infinite series, but we numerically confirmed that the sequence of partial sums converges rapidly. In the last form of Eq. (45), each term has two physical cuts on the imaginary axis; one is an upward vertical line starting from the branch point  $\tilde{q} = i(\mathcal{M}_f + \mathcal{M}_{f'})$  and the other is a downward vertical line from the branch point  $\tilde{q} = -i(\mathcal{M}_f + \mathcal{M}_{f'})$ . In the upper half-plane where the contour integration is taken, the lowest branch point is  $\tilde{q} = i(\mathcal{M}_f + \mathcal{M}_{f'})_{j=1,n=0,\alpha=0}$ .

The screening mass  $M_\xi^{\text{scr}}$  is determined as a pole of  $\chi_{\xi\xi}(0, \tilde{q}^2)$  on the imaginary  $\tilde{q}$  axis. The pole should be located below the lowest branch point:

$$M_\xi^{\text{scr}} < M_{\text{th}} \equiv (\mathcal{M}_f + \mathcal{M}_{f'})_{j=1,n=0,\alpha=0}, \quad (47)$$

where  $M_{\text{th}}$  can be regarded as ‘‘threshold mass’’ in the sense that meson is in  $q\bar{q}$  continuum states when  $M_\xi^{\text{scr}} > M_{\text{th}}$ . For  $\xi = \pi, a_0, K, \kappa$  channels, we can obtain the  $M_\xi^{\text{scr}}$  by solving the equation

$$\left[1 - 2G_\xi \Pi_\xi(0, \tilde{q}^2)\right]_{\tilde{q}=iM_\xi^{\text{scr}}} = 0, \quad (48)$$

when  $M_\xi^{\text{scr}} < M_{\text{th}}$ . As  $T$  increases,  $M_\xi^{\text{scr}}$  (pole) approaches  $M_{\text{th}}$  (the lowest branch point) from below [31, 36]. Meanwhile,  $M_{\text{th}}$  itself tends to  $2\pi T$  in the high- $T$  limit, since  $A_4^{jj}$  does to 0 in Eq. (46). Therefore,  $M_\xi^{\text{scr}}$  approaches  $2\pi T$  with respect increasing  $T$ .

Now we consider the channel mixing. The formalism on meson screening masses is the same as that on meson pole masses. Only the difference is that the external momentum is set to  $q = (0, \mathbf{q})$ . The coupled equations for the  $M_\xi^{\text{scr}}$  are

$$\det \left[ \mathbf{I} - 2\Pi_\xi(0, \tilde{q}^2) \mathbf{G}_\xi \right]_{\tilde{q}=iM_\xi^{\text{scr}}} = 0, \quad (49)$$

where  $\tilde{q} = \pm|\mathbf{q}|$ . Here note that  $M_{\text{th}} = 2(\mathcal{M}_l)_{j=1,n=0,\alpha=0}$  for  $\eta, \sigma$  mesons. For  $\eta', f_0$  mesons, we consider  $M_{\text{th}} = 2(\mathcal{M}_s)_{j=1,n=0,\alpha=0}$  as the threshold mass. Strictly speaking,  $\eta' (f_0)$  can decay into a light-quark pair by the channel mixing. However, such a contribution is unphysical for low temperature because of the color confinement and small for high temperature because of small channel mixing.

#### D. Model tuning for LQCD-data analyses

We use LQCD data of Ref. [3] for the  $M_\xi^{\text{scr}}(T)$  and of Ref. [4] for  $\Delta_{l,s}(T)$ , since the same lattice setting is taken in the two simulations. In Refs. [3, 4], the quark-mass ratio is  $m_l/m_s = 1/10$ , and the  $\pi$ -meson mass at  $T = 0$  is  $M_\pi^{\text{pole}}(0) = 176$  MeV that is slightly heavier than the experimental value 138 MeV. In model calculations, we then

change quark masses from  $(m_l, m_s) = (8 \text{ MeV}, 191 \text{ MeV})$  to  $(m_l, m_s) = (13 \text{ MeV}, 130 \text{ MeV})$  to become consistent with the lattice setting. This parameter set is tabulated as set (B) in Table II.

In LQCD simulations of Refs. [3, 4],  $T_c^X$  is measured to be 196 MeV, but the value established in state-of-art LQCD simulations of Refs. [5, 6] is  $T_c^X = 154 \pm 9$  MeV. Therefore, we rescale the values of  $T$  and  $M_\xi^{\text{scr}}$  in Refs. [3, 4] to reproduce  $T_c^X = 154 \pm 9$  MeV.

In LQCD simulations of Ref. [3] for pseudoscalar mesons ( $\eta, \eta'$ ) and scalar ones ( $\sigma, f_0$ ), the quark-line disconnected diagrams are neglected and thereby the  $\eta_{\bar{s}s}$  ( $\sigma_{\bar{s}s}$ ) channel is decoupled with the  $\eta_{\bar{l}l}$  ( $\sigma_{\bar{l}l}$ ) channel. Eventually, LQCD data are available only for  $\eta_{\bar{s}s}$ - and  $\sigma_{\bar{s}s}$ -meson screening masses. We then switch off the channel mixing in model calculations by setting  $G_{\xi_{ss}\xi_{ll}} = G_{\xi_{ll}\xi_{ss}} = 0$  for  $\xi = \eta, \sigma$ , when we analyze the LQCD data on  $\eta_{\bar{s}s}$  and  $\sigma_{\bar{s}s}$  mesons.

Particularly for  $\eta$ - and  $\eta'$ -meson masses at  $T = 0$ , it is shown in Ref. [43] that the disconnected diagrams are necessary to reproduce the experimental values, although they are neglected in finite- $T$  LQCD simulations of Ref. [3] for  $M_\xi^{\text{scr}}(T)$ . The disconnected diagrams contribute to both diagonal and off-diagonal elements of the correlation-function matrix  $\chi_\xi$  in Eq. (32), whereas the connected diagrams do to only the diagonal elements. The channel mixing induced by the off-diagonal elements is thus one of effects induced by the disconnected diagrams. We can then divide the disconnected-diagrams effects into the channel-mixing effect and the remaining disconnected-diagram effects acting on the diagonal elements of  $\chi_\xi$ . Model calculations with the parameter set (A) include the channel-mixing effect explicitly and the remaining disconnected-diagram effects implicitly, since the set (A) is so determined as to reproduce experimental data on meson pole masses at  $T = 0$ , particularly on  $M_{\eta'}^{\text{pole}}(0)$ . Hence, we can consider that model calculations with the parameter set (B) also include the channel-mixing effect explicitly and the remaining disconnected-diagram effects implicitly, whereas LQCD calculations do not have any disconnected-diagram effects. We switch off the channel mixing in model calculations to evaluate  $\eta_{\bar{s}s}$ - and  $\sigma_{\bar{s}s}$ -meson screening masses, but we should note that the remaining disconnected-diagram effects are included in model calculations implicitly.

### III. NUMERICAL RESULTS

#### A. Parameter fitting

As shown in Eqs. (3) and (4), the present model has adjustable parameters  $(T_1, b_1)$  in the KMT coupling strength  $G_D(T)$  and  $(T_2, b_2)$  in the four-quark coupling strength  $G_S(T)$ . The parameters  $(T_1, b_1)$  are determined from LQCD data associated with the  $U(1)_A$ -symmetry restoration, i.e.,  $\Delta M_{a_0,\pi}^{\text{scr}} = M_{a_0}^{\text{scr}} - M_\pi^{\text{scr}}$  in  $T > 1.1T_c^X = 170$  MeV where only the  $U(1)_A$ -symmetry breaking survives [36, 37]. Similarly, the parameters  $(T_2, b_2)$  are determined from LQCD data associated with the chiral-symmetry restoration, i.e., the pseudocritical temperature  $T_c^X = 154 \pm 9$  MeV [5, 6] and the renor-

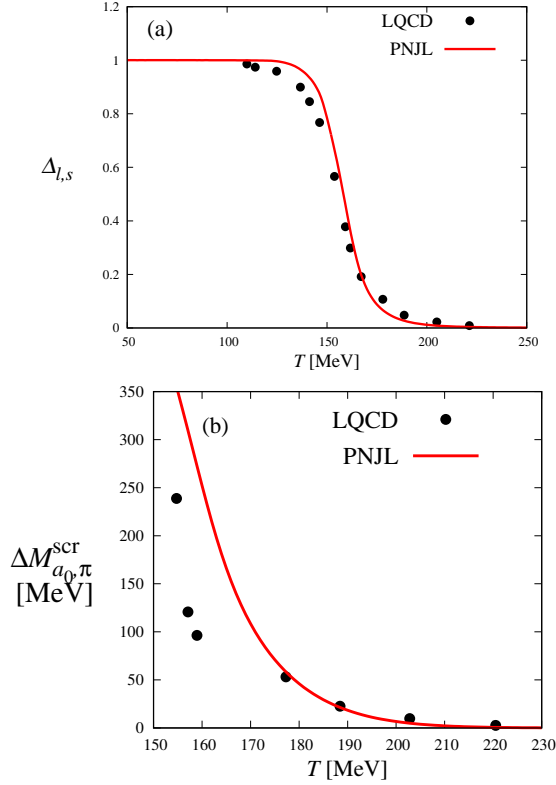


Fig. 1:  $T$  dependence of (a)  $\Delta_{l,s}$  and (b)  $\Delta M_{a_0,\pi}^{\text{scr}}$ . Model results are shown by solid lines, while LQCD data are denoted by closed circles. The parameter set (B) is taken in model calculations. LQCD data are taken from Refs. [3, 4].

malized chiral condensate  $\Delta_{l,s}(T)$  of Eq. (1).

Figure 1 shows the results of the present parameter fitting for (a)  $\Delta_{l,s}(T)$  and (b)  $\Delta M_{a_0,\pi}^{\text{scr}}(T)$ . Note that the parameter set (B) is taken in model calculations. Good agreement is seen between model results (solid lines) and LQCD data (closed circles), when  $(T_1, b_1) = (121, 43.5)$  and  $(T_2, b_2) = (131, 83.3)$  in units of MeV. These values are tabulated in Table I.

## B. Meson screening masses

We consider meson screening masses for pseudoscalar and scalar mesons and analyze LQCD data of Ref. [3], using the present model with the parameter set (B). In the model calculations the channel mixing is switched off, since the disconnected diagrams are neglected in LQCD data of Ref. [3].

Figure 2 shows  $T$  dependence of the  $M_\xi^{\text{scr}}(T)$  for (a) pseudoscalar mesons  $\xi = \pi, K, \eta_{\bar{s}s}$  and (b) scalar mesons  $\xi = a_0, \kappa, \sigma_{\bar{s}s}$ . The lines stand for model results, and the symbols correspond to LQCD data of Ref. [3]. As mentioned in Sec. II C, in model calculations the  $M_\xi^{\text{scr}}(T)$  are derivable when  $M_\xi^{\text{scr}}(T) < M_{\text{th}}$ . For the  $a_0$ -meson case, for example, the condition is satisfied for  $T > 139$  MeV. The solid line representing  $M_{a_0}^{\text{scr}}(T)$  is then drawn in  $T > 139$  MeV. The same

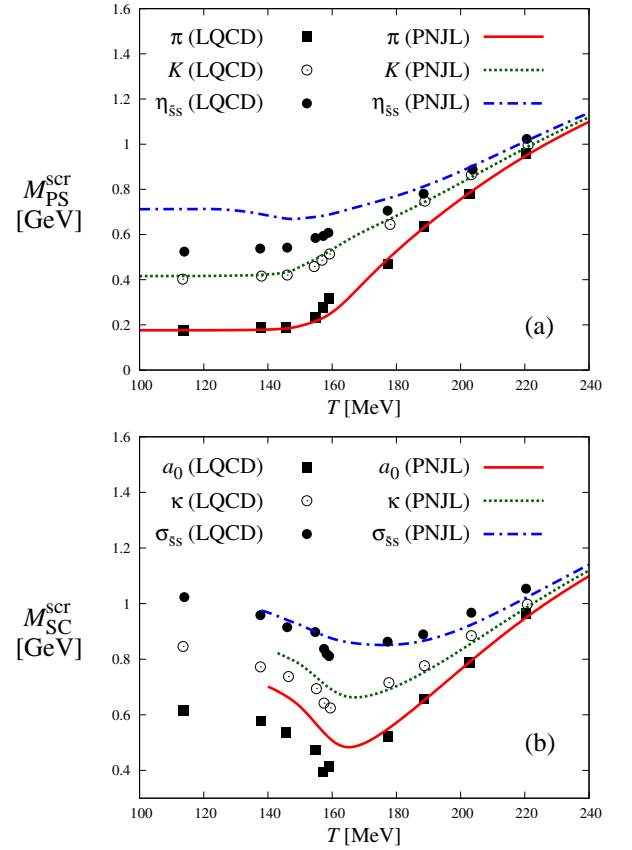


Fig. 2:  $T$  dependence of meson screening masses for (a) pseudoscalar mesons  $\pi, K, \eta_{\bar{s}s}$  and (b) scalar mesons  $a_0, \kappa, \sigma_{\bar{s}s}$ . Model results are denoted by lines and LQCD data are by symbols. The parameter set (B) is taken in model calculations. LQCD data are taken from from Ref. [3].

procedure is taken for the other lines. In both LQCD data and model results, all the meson masses tend to  $2\pi T$  with respect to increasing  $T$ ; see Sec. II C for the proof. Owing to this property, in  $T > 1.04T_c^x = 160$  MeV, model results well reproduce LQCD data for all the mesons. In  $T < 1.04T_c^x = 160$  MeV, the agreement between model results and LQCD data is good for pseudoscalar  $\pi, K$  mesons and pretty good for scalar  $a_0, \kappa, \sigma_{\bar{s}s}$  mesons. For pseudoscalar  $\eta_{\bar{s}s}$  meson, the model result overestimates LQCD data by about 10%  $\sim$  30% in  $T < 1.04T_c^x = 160$  MeV, but the deviation becomes small rapidly as  $T$  increases from 160 MeV. The deviation in  $T < 1.04T_c^x = 160$  MeV may come from the remaining disconnected-diagram effects acting on the diagonal elements of  $\chi_\xi$ . This implies that the channel-mixing effect is also important for  $\eta_{\bar{s}s}$  meson in  $T < 1.04T_c^x = 160$  MeV. This statement is confirmed with model calculations in Sec. III E. In addition, this statement is consistent with the statement of Ref. [44] that the disconnected diagrams may be suppressed at least for  $T \gg T_c^x$  by the Debye screening and the weakly interacting nature of the deconfined phase.

For later discussion, we evaluate the  $M_\xi^{\text{scr}}(T)$  also in the realistic case, taking the parameter set (A) and taking account of

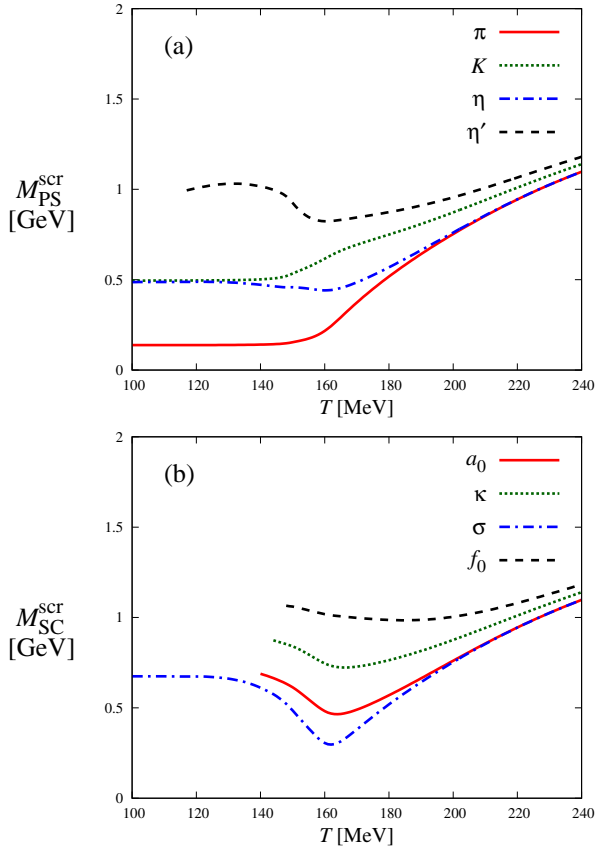


Fig. 3:  $T$  dependence of meson screening masses for (a) pseudoscalar mesons  $\pi, K, \eta, \eta'$  and (b) scalar mesons  $a_0, \kappa, \sigma, f_0$  calculated with the realistic parameter set (A). Model results are denoted by lines. In model calculations, the channel mixing is taken into account.

the channel mixing in model calculations. Figure 3 shows the results for (a) pseudoscalar mesons  $\pi, K, \eta, \eta'$  and (b) scalar mesons  $a_0, \kappa, \sigma, f_0$ . As mentioned in Fig. 2, all the meson screening masses tend to  $2\pi T$ . This property is independent of quark masses. At high  $T$ , the  $M_{\xi}^{\text{scr}}(T)$  calculated with the realistic parameter set (A) are close to those with the set (B). The difference between the former and the latter appear only in  $T < T_c^{\chi} = 154 \pm 9$  MeV.

### C. Meson pole masses

Now we predict meson pole masses in the realistic case, taking the parameter set (A) and taking account of the channel mixing in model calculations. The results are shown for pseudoscalar mesons  $\pi, K, \eta, \eta'$  in Fig. 4(a) and for scalar mesons  $a_0, \kappa, \sigma, f_0$  in Fig. 4(b). For  $\eta'$  meson, the pole mass in medium with finite  $T$  was deduced from heavy-ion collision measurements as  $M_{\eta'}^{\text{pole}}(T) = 340_{-245}^{+375}$  MeV [1]. In the analyses,  $T = 177$  MeV is taken as the default value and  $T$  is varied systematically between 140 and 220 MeV. We then denote the experimental data [1] by the rectangle ( $140 \text{ MeV} \leq T \leq$

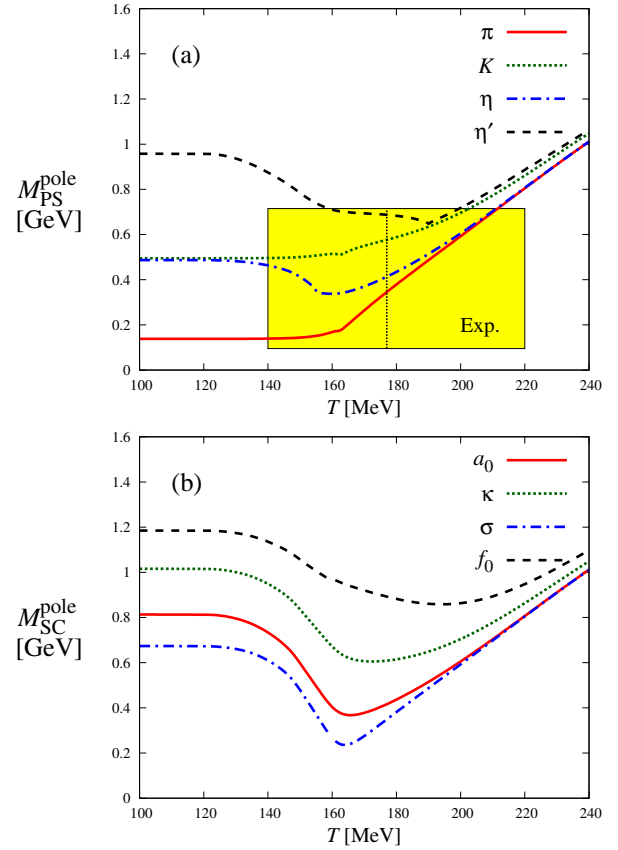


Fig. 4: Model prediction on  $T$  dependence of meson pole masses for (a) pseudoscalar mesons  $\pi, K, \eta, \eta'$  and (b) scalar mesons  $a_0, \kappa, \sigma, f_0$ . In model calculations, the parameter set (A) is taken and the channel mixing is taken into account. Model results are denoted by lines. For  $\eta'$  meson in panel (a), the experimental data [1] is shown by the rectangle with the thin dotted vertical line  $T = 177$  MeV; see the text for the explanation.

220 MeV,  $95 \text{ MeV} \leq M_{\eta'}^{\text{pole}} \leq 715 \text{ MeV}$ ) with the thin dotted vertical line standing for the default value  $T = 177$  MeV. The model result is consistent with the experimental data. In general,  $M_{\xi}^{\text{pole}}$  is not smooth when the quark-pair production threshold is opened. This threshold effect is seen at  $T = 190$  MeV, e.g., for  $\eta'$  meson.

As shown later in Sec. III E, the channel mixing is negligible for  $\eta'$  meson in  $T > 160$  MeV, indicating that  $\eta'$  meson is purely the  $\bar{s}s$  state there. This result supports the ansatz in experimental analyses that  $\eta'$  meson behaves just like a free particle in medium after it is produced.

### D. Relation between pole and screening masses

Figure 5 shows  $T$  dependence of the difference  $M_{\xi}^{\text{scr}}(T) - M_{\xi}^{\text{pole}}(T)$  for (a) pseudoscalar mesons  $\pi, K, \eta, \eta'$  and (b) scalar mesons  $a_0, \kappa, \sigma, f_0$ , where the parameter set (A) is taken and the channel mixing is taken into account in model

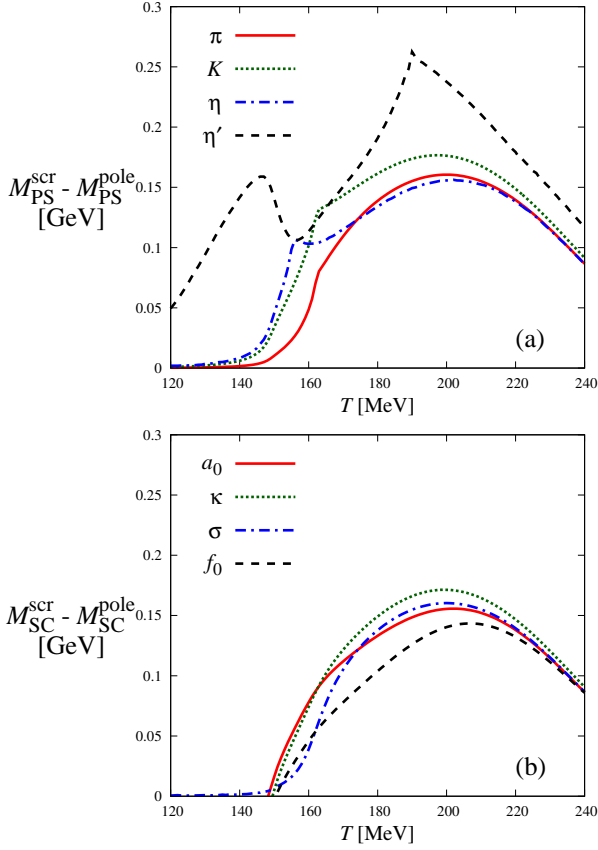


Fig. 5: Difference between screening and pole masses for (a) pseudoscalar mesons  $\pi$ ,  $K$ ,  $\eta$ ,  $\eta'$  and (b) scalar mesons  $a_0$ ,  $\kappa$ ,  $\sigma$ ,  $f_0$ . Model results are denoted by lines. In model calculations, the parameter set (A) is taken and the channel mixing is taken into account.

calculations, whenever  $T$  dependence of the difference is not smooth, it is due to the threshold effect. For pseudoscalar mesons, the difference tends to become larger for heavier meson. For scalar mesons, meanwhile, the difference is universal approximately:

$$M_{\xi}^{\text{scr}}(T) - M_{\xi}^{\text{pole}}(T) \approx M_{\xi'}^{\text{scr}}(T) - M_{\xi'}^{\text{pole}}(T) \quad (50)$$

for  $\xi \neq \xi'$ . The deviation is about 35 MeV at  $T \approx 200$  MeV. If  $M_{\xi}^{\text{scr}}(T)$ ,  $M_{\xi'}^{\text{scr}}(T)$  and  $M_{\xi'}^{\text{pole}}(T)$  are obtained with LQCD simulations, one can estimate  $T$  dependence of  $M_{\xi}^{\text{pole}}(T)$  by using Eq. (50).

Next, the relation between  $M_{\xi}^{\text{pole}}(T)$  and  $M_{\xi}^{\text{scr}}(T)$  is considered through the ratios  $M_{\xi}^{\text{pole}}(T)/M_{\xi'}^{\text{pole}}(T)$  and  $M_{\xi}^{\text{scr}}(T)/M_{\xi'}^{\text{scr}}(T)$ , where  $\xi'$  is assumed to be a scalar (pseudoscalar) meson when  $\xi$  is a scalar (pseudoscalar) meson. The identity

$$\frac{M_{\xi}^{\text{pole}}(T)}{M_{\xi'}^{\text{pole}}(T)} = \frac{M_{\xi}^{\text{scr}}(T)}{M_{\xi'}^{\text{scr}}(T)} \quad (51)$$

is satisfied at both  $T = 0$  and  $\infty$ . The identity at  $T = 0$  comes from the fact that  $M_{\xi}^{\text{scr}}(0) = M_{\xi}^{\text{pole}}(0)$  for any me-

son. The identity at  $T = \infty$  can be proven as follows. As mentioned in Sec. II C, in the large- $T$  limit all the  $M_{\xi}^{\text{scr}}(T)$  tend to  $2\pi T$ . Therefore, the ratio  $M_{\xi}^{\text{scr}}/M_{\xi'}^{\text{scr}}$  becomes 1 in the limit. Similarly, the ratio  $M_{\xi}^{\text{pole}}/M_{\xi'}^{\text{pole}}$  approaches 1 with respect to increasing  $T$  as a consequence of the *effective*  $SU(3)_V$ -symmetry restoration. The symmetry is broken by the fact  $m_s \neq m_l$  in vacuum, but it is restored *effectively* at high  $T$  because the symmetry breaking is the order of  $(m_s - m_l)/T$  there; precisely speaking, for the flavor-singlet states, the symmetry is broken also by the quark-line disconnected diagrams, but the diagrams are suppressed by the Debye screening and the weakly interacting nature at high  $T$  [44].

Figure 6 shows the ratios as a function of  $T$  for (a) pseudoscalar mesons ( $\xi = K, \eta, \eta', \xi' = \pi$ ) and (b) scalar mesons ( $\xi = \kappa, \sigma, f_0, \xi' = a_0$ ). Qualitatively, the two ratios have similar  $T$  dependence each other for both pseudoscalar and scalar mesons: Namely,

$$\frac{M_{\xi}^{\text{pole}}(T)}{M_{\xi'}^{\text{pole}}(T)} \simeq \frac{M_{\xi}^{\text{scr}}(T)}{M_{\xi'}^{\text{scr}}(T)}. \quad (52)$$

Quantitatively, the relation (52) is well satisfied within 20% error for pseudoscalar and scalar mesons. The relation is useful, because it allows us to estimate  $M_{\xi}^{\text{pole}}(T)$  for lighter  $\xi$ -meson from  $M_{\xi'}^{\text{pole}}(T)$  for heavier  $\xi'$ -meson and  $M_{\xi}^{\text{scr}}(T)/M_{\xi'}^{\text{scr}}(T)$  that may be obtainable with state-of-art LQCD simulations.

## E. Discussion

$T$  dependence of the channel-mixing effect is investigated within model calculations. The parameter set (B) is taken in model calculations. In Fig. 7(a), the thin and thick solid lines denote the results of model calculations with the channel mixing for screening masses of  $\eta$  and  $\eta'$  mesons, respectively. Note that the lines are drawn when the condition  $M_{\xi}^{\text{scr}}(T) < M_{\text{th}}$  is satisfied. When the channel mixing is switched off, the thin and thick solid lines are changed into the thin and thick dashed lines that stand for screening masses of  $\eta_{ll}$  and  $\eta_{\bar{s}s}$  channels, respectively. As expected in Sec. III B, the channel-mixing effect is large for  $\eta$ - and  $\eta'$ -meson screening masses in  $T < 1.04T_c^{\chi} = 160$  MeV. This is a result of the fact that the mass difference between the thin and thick dashed lines is small there; for example, the difference is 113 MeV at  $T = 140$  MeV. For  $T > 1.04T_c^{\chi} = 160$  MeV, the channel-mixing effect is negligible, since  $G_{\eta_{\bar{s}s}\eta_{ll}} = G_{\eta_{ll}\eta_{\bar{s}s}} = G_D(T)\sigma_l/\sqrt{2}$  is quite small in Eq. (34) because of  $\sigma_l \approx 0$ . In Fig. 7(b), the thin and thick solid lines stand for the results of model calculations with the channel mixing for screening masses of  $\sigma$  and  $f_0$  mesons, respectively, while the thin and thick dashed lines correspond to the results of model calculations without the channel mixing for screening masses of  $\sigma_{ll}$  and  $\sigma_{\bar{s}s}$  channels, respectively. In the case of  $\sigma$  and  $f_0$  mesons, the channel-mixing effect is negligible for any  $T$ . This is because the mass difference between the thin and thick dashed lines is large in

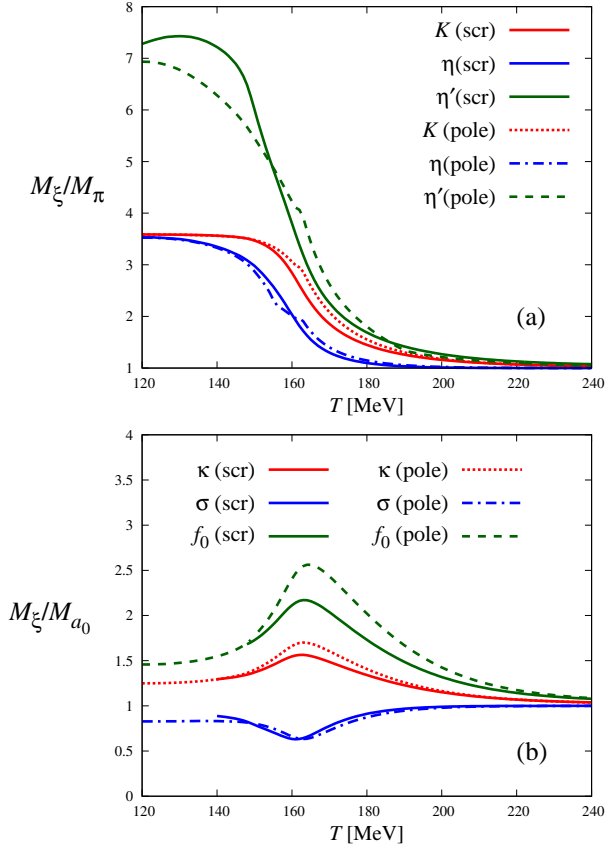


Fig. 6:  $T$  dependence of  $M_{\xi}^{\text{pole}}/M_{\xi'}^{\text{pole}}$  and  $M_{\xi}^{\text{scr}}/M_{\xi'}^{\text{scr}}$  for (a) pseudoscalar mesons ( $\xi = K, \eta, \eta', \xi' = \pi$ ) and (b) scalar mesons ( $\xi = \kappa, \sigma, f_0, \xi' = a_0$ ). The ratios  $M_{\xi}^{\text{scr}}/M_{\xi'}^{\text{scr}}$  are denoted by solid lines, and the ratios  $M_{\xi}^{\text{pole}}/M_{\xi'}^{\text{pole}}$  are by dotted, dashed and dot-dashed lines. In model calculations, the parameter set (A) is taken and the channel mixing is taken into account.

$T < 1.04T_c^x = 160$  MeV (e.g., the difference is 335 MeV at  $T = 140$  MeV) and  $G_{\sigma_{\bar{s}s}\sigma_{\bar{l}l}} = G_{\sigma_{\bar{l}l}\sigma_{\bar{s}s}} = -G_D(T)\sigma_l/\sqrt{2} \approx 0$  because of  $\sigma_l \approx 0$  in  $T > 1.04T_c^x = 160$  MeV. Consequently, the channel mixing as the characteristics of the disconnected diagrams is important only for  $\eta$ - and  $\eta'$ -meson screening masses in  $T < 1.04T_c^x = 160$  MeV. Also for  $\eta$ - and  $\eta'$ -meson pole masses, we can take the same conclusion.

#### IV. SUMMARY

We have proposed a practical effective model by introducing  $T$ -dependent coupling strengths,  $G_S(T)$  and  $G_D(T)$ , to four-quark and six-quark KMT interactions in the 2+1 flavor PNJL model.  $T$  dependence of  $G_D(T)$  is determined from LQCD data [3] on  $\Delta M_{a_0, \pi}^{\text{scr}}(T)$  in  $T > 1.1T_c^x = 170$  MeV where only the  $U(1)_A$ -symmetry breaking survives. Similarly,  $T$  dependence of  $G_S(T)$  is determined from LQCD data associated with the chiral-symmetry restoration, i.e., the renormalized chiral condensate  $\Delta_{l,s}(T)$  [4] and the pseud-

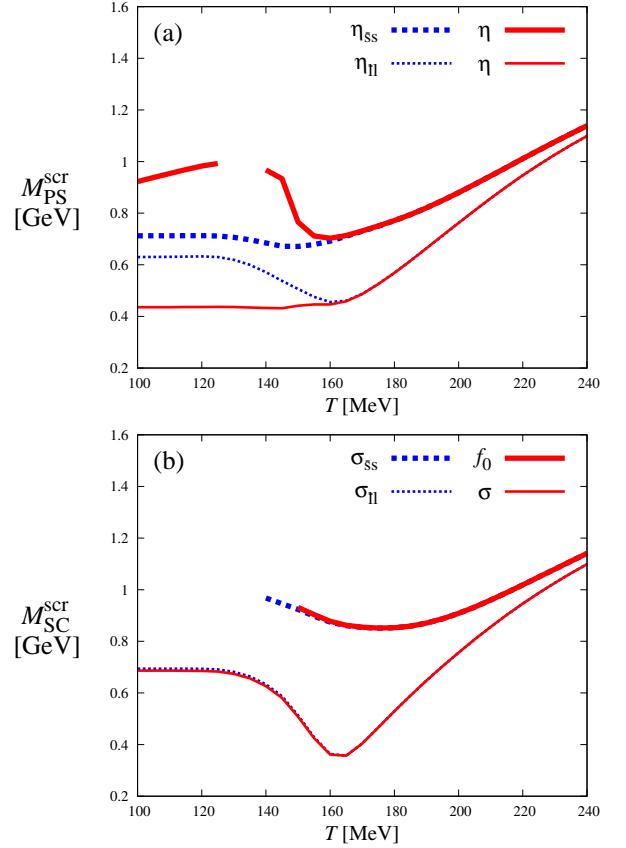


Fig. 7:  $T$  dependence of channel-mixing effects on (a)  $\eta$ - and  $\eta'$ -meson screening masses and (b)  $\sigma$ - and  $f_0$ -meson screening masses. In panel (a) (panel (b)), the thin and thick solid lines denote screening masses of  $\eta$  and  $\eta'$  ( $\sigma$  and  $f_0$ ) mesons, respectively, and the thin and thick dashed lines correspond to screening masses of  $\eta_{\bar{l}l}$  and  $\eta_{\bar{s}s}$  ( $\sigma_{\bar{l}l}$  and  $\sigma_{\bar{s}s}$ ) channels, respectively. The parameter set (B) is taken in model calculations.

ocritical temperature  $T_c^x = 154 \pm 9$  MeV [5, 6] of chiral transition. In LQCD simulations of Ref. [3, 4], the lattice setting is that  $m_l/m_s = 1/10$  and  $M_{\pi}^{\text{pole}}(0) = 176$  MeV. In model calculations,  $m_l$  and  $m_s$  are slightly changed from the realistic parameter set (A) of  $M_{\pi}^{\text{pole}}(0) = 138$  MeV and  $M_K^{\text{pole}}(0) = 495$  MeV so as to become consistent with the lattice setting. This parameter set is referred to as set (B).

The present model with the parameter set (B) reproduces LQCD data [3] on  $M_{\xi}^{\text{scr}}(T)$  for both pseudoscalar mesons  $\pi, K, \eta_{\bar{s}s}$  and scalar mesons  $a_0, \kappa, \sigma_{\bar{s}s}$  in  $T > 1.04T_c^x = 160$  MeV. Meanwhile, in  $T < 1.04T_c^x = 160$  MeV, the agreement between model results and LQCD data is good for pseudoscalar  $\pi, K$  mesons and pretty good for scalar  $a_0, \kappa, \sigma_{\bar{s}s}$  mesons. For  $\eta_{\bar{s}s}$  meson, the model result overestimates LQCD data by about 10%  $\sim$  30% in  $T < 1.04T_c^x = 160$  MeV, but the deviation decreases rapidly as  $T$  increases from 160 MeV.

In finite- $T$  LQCD simulations of Ref. [3], the disconnected diagrams are neglected when  $M_{\eta_{\bar{s}s}}^{\text{scr}}(T)$  is calculated. As a consequence of this approximation, the  $\eta_{\bar{s}s}$  channel is decoupled with the  $\eta_{\bar{l}l}$  channel. We then divide the disconnected-

diagram effects into the channel-mixing effect and the remaining disconnected-diagram effects acting on the diagonal elements of the correlation-function matrix  $\chi_\xi$ . The model calculation includes the remaining disconnected-diagram effects implicitly, even if the channel mixing is switched off. The deviation between model calculations and LQCD data for  $\eta_{\bar{s}s}$  meson in  $T < 1.04T_c^x = 160$  MeV may stem from the remaining disconnected-diagram effects implicitly included in model calculations.

Using this practical effective model with the realistic parameter set (A), we have predicted meson pole masses  $M_\xi^{\text{pole}}(T)$  for pseudoscalar mesons  $\pi, K, \eta, \eta'$  and scalar mesons  $a_0, \kappa, \sigma, f_0$ . This prediction makes it possible to compare the  $M_\xi^{\text{pole}}(T)$  evaluated from LQCD data with the corresponding experimental results directly. In fact, we have shown that for  $\eta'$  meson the model prediction is consistent with the experimental value [1] at finite  $T$  measured in heavy-ion collisions. If experimental data are not available for  $M_\xi^{\text{pole}}(T)$  of interest, such a prediction may be helpful in experimental analyses.

We have shown that the relation  $M_\xi^{\text{scr}}(T) - M_\xi^{\text{pole}}(T) \approx M_{\xi'}^{\text{scr}}(T) - M_{\xi'}^{\text{pole}}(T)$  is pretty good when  $\xi$  and  $\xi'$  are scalar mesons, and have pointed out that the relation  $M_\xi^{\text{scr}}(T)/M_{\xi'}^{\text{scr}}(T) \approx M_\xi^{\text{pole}}(T)/M_{\xi'}^{\text{pole}}(T)$  is well satisfied within 20% error when  $\xi$  and  $\xi'$  are pseudoscalar mesons and also when  $\xi$  and  $\xi'$  are scalar mesons. These relations may be useful to estimate  $M_\xi^{\text{pole}}$  for lighter  $\xi$ -meson from  $M_{\xi'}^{\text{pole}}$  and  $M_{\xi'}^{\text{scr}}$  for heavier  $\xi'$ -meson that may be obtainable with state-of-art LQCD simulations.

We have also found that the channel mixing as the characteristics of the disconnected diagrams is important only for  $\eta$ - and  $\eta'$ -meson masses in  $T < 1.04T_c^x = 160$  MeV. This indicates that  $\eta'$  meson is purely the  $\bar{s}s$  state in  $T \gtrsim 1.04T_c^x = 160$  MeV. This result supports the ansatz in experimental analyses that  $\eta'$  meson behaves just like a free particle in medium

after it is produced.

## Acknowledgments

M. I, H. K., and M. Y. are supported by Grants-in-Aid for Scientific Research ( No. 27-3944, No. 26400279 and No. 26400278) from the Japan Society for the Promotion of Science (JSPS). The authors thank to J. Takahashi, Y. Maezawa and M. Oka for useful comments.

## Appendix A: Difficulty of meson pole-mass calculations in LQCD simulations at finite $T$

In general, the meson pole mass  $M_\xi^{\text{pole}}$  and its decay width  $\Gamma_\xi$  are determined from energy ( $\omega$ ) dependence of the spectral function  $\rho_{\xi\xi}(\omega, \mathbf{p}, T)$ , where the spatial momentum  $\mathbf{p}$  is set to zero when we calculate the pole mass. In the Matsubara formalism,  $\rho_{\xi\xi}(\omega, \mathbf{p}, T)$  is related to the mesonic correlation function  $\mathcal{G}_{\xi\xi}(\tau, \mathbf{p}, T)$  as

$$\mathcal{G}_{\xi\xi}(\tau, \mathbf{p}, T) = \int_0^\infty d\omega \rho_{\xi\xi}(\omega, \mathbf{p}, T) K(\omega, \tau, T), \quad (\text{A1})$$

$$K(\omega, \tau, T) = \frac{\cosh[\omega(\tau - 1/2T)]}{\sinh(\omega/2T)}, \quad (\text{A2})$$

where  $\tau$  represents imaginary time satisfying  $0 \leq \tau \leq 1/T$ . If the  $\mathcal{G}_{\xi\xi}(\tau, \mathbf{p}, T)$  is known, the spectral function  $\rho_{\xi\xi}(\omega, \mathbf{p}, T)$  can be obtained from the  $\mathcal{G}_{\xi\xi}$  by solving the integral equation (A1) for  $\rho_{\xi\xi}$ . In LQCD simulations at finite  $T$ , the  $\mathcal{G}_{\xi\xi}(\tau, \mathbf{p}, T)$  is obtained only for a limited number of  $\tau$  up to  $1/T$ . In general, the number is too small to construct  $\rho_{\xi\xi}$  as a continuous function of  $\omega$ .

- 
- [1] T. Csörgő, R. Vértési, and J. Sziklai, Phys. Rev. Lett. **105**, 182301 (2010).  
[2] L. Adamczyk *et al.* (STAR Collaboration), Phys. Rev. Lett. **113**, 022301 (2014).  
[3] M. Cheng, S. Datta, A. Francis, J. van der Heide, C. Jung, O. Kaczmarek, F. Karsch, and E. Laermann *et al.*, Eur. Phys. J. C **71**, 1564 (2011) [arXiv: 1010.1216].  
[4] M. Cheng, N. H. Christ, S. Datta, J. van der Heide, C. Jung, F. Karsch, O. Kaczmarek, and E. Laermann *et al.*, Phys. Rev. D **77**, 014511 (2008).  
[5] S. Borsanyi *et al.* (Wuppertal-Budapest Collaboration), J. High Energy Phys. **09** (2010) 073 [arXiv:1005.3508].  
[6] A. Bazavov *et al.* (HotQCD Collaboration), Phys. Rev. D **85**, 054503 (2012) [arXiv: 1111.1710].  
[7] Y. Aoki, G. Endrődi, Z. Fodor, S. D. Katz, and K. K. Szabó, Nature(London) **443**, 675 (2006).  
[8] S. P. Klevansky, Rev. Mod. Phys. **64**, 649 (1992); T. Hatsuda, and T. Kunihiro, Phys. Rep. **247**, 221 (1994); M. Buballa, Phys. Rep. **407**, 205 (2005).  
[9] P. N. Meisinger, and M. C. Ogilvie, Phys. Lett. B **379**, 163 (1996).  
[10] A. Dumitru, and R. D. Pisarski, Phys. Rev. D **66**, 096003 (2002).  
[11] K. Fukushima, Phys. Lett. B **591**, 277 (2004); K. Fukushima, Phys. Rev. D **77**, 114028 (2008); Phys. Rev. D **78**, 114019 (2008).  
[12] P. Costa, M. C. Ruivo, C. A. de Sousa, and Yu. L. Kalinovsky, Phys. Rev. D **71**, 116002 (2005).  
[13] S. K. Ghosh, T. K. Mukherjee, M. G. Mustafa, and R. Ray, Phys. Rev. D **73**, 114007 (2006).  
[14] E. Megias, E. R. Arriola, and L. L. Salcedo, Phys. Rev. D **74**, 065005 (2006).  
[15] C. Ratti, M. A. Thaler, and W. Weise, Phys. Rev. D **73**, 014019 (2006).  
[16] M. Ciminale, R. Gatto, G. Nardulli, and M. Ruggieri, Phys. Lett. B **657**, 64 (2007); M. Ciminale, R. Gatto, N. D. Ippolito, G. Nardulli, and M. Ruggieri, Phys. Rev. D **77**, 054023 (2008).  
[17] C. Ratti, S. Rößner, M. A. Thaler, and W. Weise, Eur. Phys. J. C **49**, 213 (2007).  
[18] S. Rößner, C. Ratti, and W. Weise, Phys. Rev. D **75**, 034007

- (2007).
- [19] H. Hansen, W. M. Alberico, A. Beraudo, A. Molinari, M. Nardi, and C. Ratti, *Phys. Rev. D* **75**, 065004 (2007).
- [20] C. Sasaki, B. Friman, and K. Redlich, *Phys. Rev. D* **75**, 074013 (2007).
- [21] B. -J. Schaefer, J. M. Pawłowski, and J. Wambach, *Phys. Rev. D* **76**, 074023 (2007).
- [22] K. Kashiwa, H. Kouno, M. Matsuzaki, and M. Yahiro, *Phys. Lett. B* **662**, 26 (2008).
- [23] P. Costa, M. C. Ruivo, C. A. de Sousa, H. Hansen, and W. M. Alberico, *Phys. Rev. D* **79**, 116003 (2009).
- [24] M. C. Ruivo, M. Santos, P. Costa, and C. A. de Sousa, *Phys. Rev. D* **85**, 036001 (2012).
- [25] Y. Sakai, T. Sasaki, H. Kouno, and M. Yahiro, *Phys. Rev. D* **82**, 076003 (2010).
- [26] T. Sasaki, Y. Sakai, H. Kouno, and M. Yahiro, *Phys. Rev. D* **84**, 091901(R) (2011).
- [27] M. D'Elia, and F. Sanfilippo, *Phys. Rev. D* **80**, 111501(R) (2009).
- [28] P. de Forcrand, and O. Philipsen, *Phys. Rev. Lett.* **105**, 152001 (2010) [arXiv:1004.3144].
- [29] J. B. Kogut, and D. K. Sinclair, *Phys. Rev. D* **70**, 094501 (2004).
- [30] M. C. Ruivo, P. Costa, and C. A. de Sousa, *Phys. Rev. D* **86**, 116007 (2012).
- [31] M. Ishii, T. Sasaki, K. Kashiwa, H. Kouno, and M. Yahiro, *Phys. Rev. D* **89**, 071901(R) (2014). [arXiv:1312.7424].
- [32] M. Kobayashi, and T. Maskawa, *Prog. Theor. Phys.* **44**, 1422 (1970); M. Kobayashi, H. Kondo, and T. Maskawa, *Prog. Theor. Phys.* **45**, 1955 (1971).
- [33] G. 't Hooft, *Phys. Rev. Lett.* **37**, 8 (1976); *Phys. Rev. D* **14**, 3432 (1976); **18**, 2199(E) (1978).
- [34] R. D. Pisarski, and L. G. Yaffe, *Phys. Lett. B* **97**, 110 (1980).
- [35] E. V. Shuryak, *Comments Nucl. Part. Phys.* **21**, 235 (1994) [arXiv:9310253].
- [36] M. Ishii, K. Yonemura, J. Takahashi, H. Kouno, and M. Yahiro, *Phys. Rev. D* **93**, 016002 (2016). [arXiv:1504.04463].
- [37] T. Bhattacharya *et al.* (HotQCD Collaboration), *Phys. Rev. Lett.* **113**, 082001 (2014) [arXiv: 1402.5175].
- [38] W. Florkowski, *Acta Phys. Pol. B* **28**, 2079 (1997) [arXiv:9701223].
- [39] W. Pauli, and F. Villars, *Rev. Mod. Phys.* **21**, 434 (1949).
- [40] K. A. Olive (Particle Data Group), *Chin. Phys. C* **38**, 090001 (2014).
- [41] F. E. Close, *An Introduction to Quarks and Partons* (Academic Press, New York, 1997); L. Brekke and J. L. Rosner, *Nucl. Part. Phys.* **18**, (1988) 347.
- [42] C. Itzykson, and J. -B. Zuber, 1980, *Quantum Field Theory* (McGraw-Hill, New York)
- [43] N. H. Christ *et al.* (RBC and UKQCD Collaboration), *Phys. Rev. Lett.* **105**, 241601 (2010).
- [44] A. Bazavov *et al.* (HotQCD Collaboration), *Phys. Rev. D* **86**, 094503 (2012).